Pergamon

Journal of Structural Geology, Vol. 17, No. 5, pp. 647 to 662, 1995

0191-8141/95 $9.50 + 0.00

0191-8141(94)00087-5

Thrust sheet rotation and out-of-plane strains associated with oblique ramps: An example from the Wyoming salient, U.S.A.

TED G. APOTRIA*

Center for Tectonophysics and Department of Geology, Texas A&M University, College Station, TX 77843, U.S.A.

(*Received* 8 *July* 1993; *accepted in revised form* 1 *August* 1994)

Abstract—Movement over oblique thrust ramps results in local thrust sheet rotation and principal strains which deviate from the transport plane. Resulting folds, faults and deformation fabrics are superposed on those associated with displacement on frontal ramps. The South Fork thrust, a hangingwall imbricate of the Absaroka thrust sheet, SW Wyoming, has a steeply-dipping (~70°), small-displacement (~300 m), oblique ramp in the hangingwall and footwall, which makes an angle of 25° to the regional transport direction. Two penetrative deformation events are recorded by folding, stylolitic cleavage, and calcite twinning strains in the deformed hangingwall and footwall. The first is E- to SE-directed layer-parallel shortening prior to or during motion of the Absaroka thrust sheet. The second event indicates NE-directed shortening unique to the oblique ramp, at a high angle to ramp strike. At the trailing frontal ramp-oblique ramp intersection, folds in the footwall and normal faults in the hangingwall reflect local strike-parallel shortening and extension, due to out-of-plane deflection of the wallrock during displacement. The out-of-plane strains are consistent with those predicted by kinematic and mechanical models. In the hangingwall of the oblique ramp, cross-strike fractures and bedding are rotated ~30° counterclockwise about a vertical axis with respect to structural domains to the north and south due to differential displacement on the South Fork thrust. Stylolitic cleavage and calcite strains unique to the oblique ramp show a similar change in attitude indicating the rotation was the latest recorded stage of deformation.

In general, if an oblique ramp is shallowly-dipping, the hangingwall may move from the lower flat, up the ramp, and onto the upper flat. If an oblique ramp has a steep dip, as in the case of the South Fork thrust, relatively greater sliding and bending resistance may impede displacement up the ramp and upper flat. Further transport of the thrust sheet is then accommodated by footwall deformation and hangingwall rotation.

INTRODUCTION

Fold-thrust belts are comprised of faults which are linked in a three-dimensional network of ramps and flats. Frontal, lateral and oblique ramps strike perpendicular, parallel and oblique, respectively, to the tectonic transport direction (Fig. 1).

What is the deformation response of a thrust sheet resulting from motion over a footwall oblique ramp? As the hangingwall negotiates an oblique ramp, do material particles remain within the tectonic transport plane (*xz*, Fig. 1), or are they deflected resulting in out-of-plane deformation? What is the orientation of the principal stresses and strains with respect to the local material transport direction? Is the footwall rigid or deformable? Is thrust sheet rotation involved in the deformation? These questions are addressed primarily on the basis of field observations of macroscopic (map-scale folds and faults), mesoscopic (folds, fractures and stylolitic cleavage), and microscopic structures (calcite twin lamellae). The observations are coupled with insights from kinematic and mechanical modelling studies (e.g. Apotria 1990, Apotria *et al.* 1992, Wilkerson *et al.* 1992) in an effort to explain the deformation style associated with oblique ramps.

Oblique ramps are scale independent and have several structural associations. Oblique ramps transfer displacement (Gardener & Spang 1973, Pfiffner 1981, Goldberg 1984, Mitra 1988), accommodate differential displacement (Moffat & Spang 1984), or displacement termination (Boyer & Elliot 1982, Butler 1982, Lageson 1984).

Oblique ramps localize anomalous deformation of the hangingwall and generally violate the assumption of plane-strain deformation (Wheeler 1980, Coward & Kim 1981, Butler 1982, McCaskey 1982, Mitra & Yonkee 1985, Evans 1989). Folds over oblique ramps are generally oblique to the regional trend and are linked to frontal ramp folds at potentially complex intersections (Wilkerson *et al.* 1991, Apotria *et al.* 1992). Obliquely oriented reverse and normal faults and zones of intensely fractured and cleaved rock suggest oblique ramps influence hydrocarbon trap and reservoir continuity (Boyer 1985).

Recent studies have documented thrust sheet rotation associated with oblique ramps, in which the sense of rotation depends on the strike of the oblique ramp with respect to the transport direction (Dinares *et al.* 1992, Jolly & Sheriff 1992).

GEOLOGY OF THE STUDY AREA

The South Fork thrust fault is located in the hangingwall of the Absaroka thrust sheet in SW Wyoming at about 42°10′N latitude, 110°35′ longitude (Fig. 2). The

*Present address: Exxon Production Research Company, P.O. Box 2189, Houston, TX 77252-2189, U.S.A.

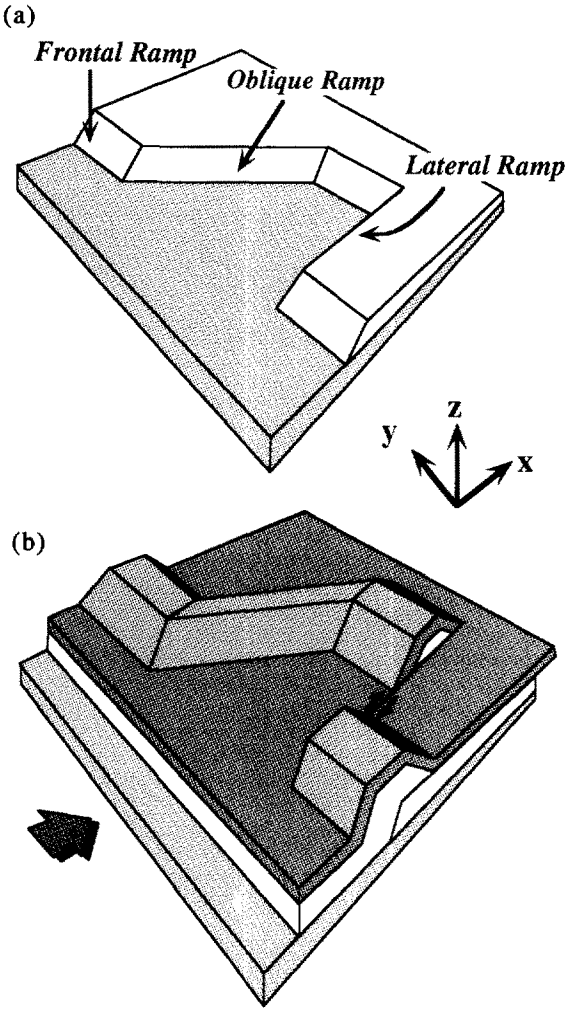

Fig. 1. (a) Footwall geometry. Frontal ramps strike perpendicular to the transport direction (*xz*-plane). (b) Simplified view of hangingwall structure assuming plane strain and a rigid footwall.

structure is well documented on a regional scale (Rubey *et al.* 1980, Oriel & Platt 1980), and is clearly visible on the Wyoming state map (Love & Christiansen 1985).

The area was mapped in this study at a scale of 1:12,000 and lies within T25N, R116W (Figs. 2 and 3). Directly to the west is the Fossil Basin, a piggyback basin of the Absaroka thrust sheet (Lamerson 1982). The Lazeart syncline in the hangingwall of the Hogsback thrust is to the east.

Tectonic framework

The Idaho–Wyoming–Utah thrust belt salient is cut by six major W-dipping thrust faults, several minor imbricates, and late listric normal faults. The geometry of the major structures is well documented (Royse *et al.* 1975, Dixon 1982, Lamerson 1982, Coogan 1992). From west to east, the major thrust faults are: Paris-Willard, Meade, Crawford, Absaroka, Darby-Hogsback, and Prospect (Fig. 2). The Paris-Willard thrust moved in latest Jurassic–Early Cretaceous (Neocomian), the Meade and Crawford system moved in the Middle Cretaceous (Albian and Conacian, respectively), the Absaroka thrust moved in Pre-Mid Santonian to Pre-Campanian-Maestrichtian, the Darby-Hogsback moved in late Paleocene–Early Eocene (Selandian), and the youngest thrust, the Prospect, moved in Early Eocene (Ypresian) (Armstrong & Oriel 1965, Royse *et al.* 1975, Wiltschko & Dorr 1983).

The South Fork thrust fault is one of several imbricates of the Absaroka thrust, including from east to west, South Fork thrust, Commissary thrust, Beaver Creek thrust, and Tunp thrust (Rubey *et al.* 1980). Based on seismic and well control, Lamerson (1982) interprets the Commissary thrust as an imbricate of the Absaroka thrust, and the Tunp as an imbricate to the Commissary thrust, implying a westward-breaking sequence of imbrication. Available data do not constrain the age of the South Fork thrust, although the results of this study suggest it is close in age to Absaroka and Commissary displacement.

Cenozoic age normal faults are documented in the hangingwall of the Tunp thrust, west of this study area. Where mapped, these faults generally strike N–S (Lamerson 1982). Normal faults mapped near the South Fork oblique ramp strike E–W. Although their age is not rigorously constrained in this study, their orientation, minor offset, and association with the South Fork thrust, suggest they are associated with thrusting and are not Cenozoic faults.

MACROSCOPIC STRUCTURES

At the southern edge of the study area, the Absaroka thrust strikes N–S and carries Mississippian Madison Limestone in its hangingwall (Fig. 3). Northward, the Absaroka thrust trace abruptly changes trend to N60°W, changes stratigraphic position in the hangingwall to the Permian Phosphoria Formation, then regains a north–south trend along strike in the Pennsylvanian-Permian Wells Formation. The South Fork thrust is parallel to the Absaroka thrust to the south, then cuts up-section northward from the Wells Formation to the Jurassic Preuss Sandstone (Fig. 3). Cross-sections based on well and seismic data confirm that the Commissary thrust soles into a shallower detachment and that it does not branch with the Absaroka thrust at the level of the Commissary detachment (Lamerson 1982, Coogan 1992). The oblique ramp trace of the South Fork thrust has an azimuth of N65°W, making an angle of 25° to the regional east–west transport direction. In the hangingwall, the oblique ramp is marked by a change in the strike and dip of bedding from N0°E/40°W to N30°W/60°SW. From west to east, the sense of offset varies from right lateral, to a point of zero apparent offset, to a left lateral offset near the leading oblique ramp–frontal ramp intersection (Fig. 3).

The dip of the South Fork thrust along the length of the oblique ramp is not known precisely from well or seismic data, but can be inferred from the map pattern (Apotria 1990). Estimated dip magnitudes of the South Fork oblique ramp range from 58°SW to 82°SW. Although not rigorously constrained, the oblique ramp

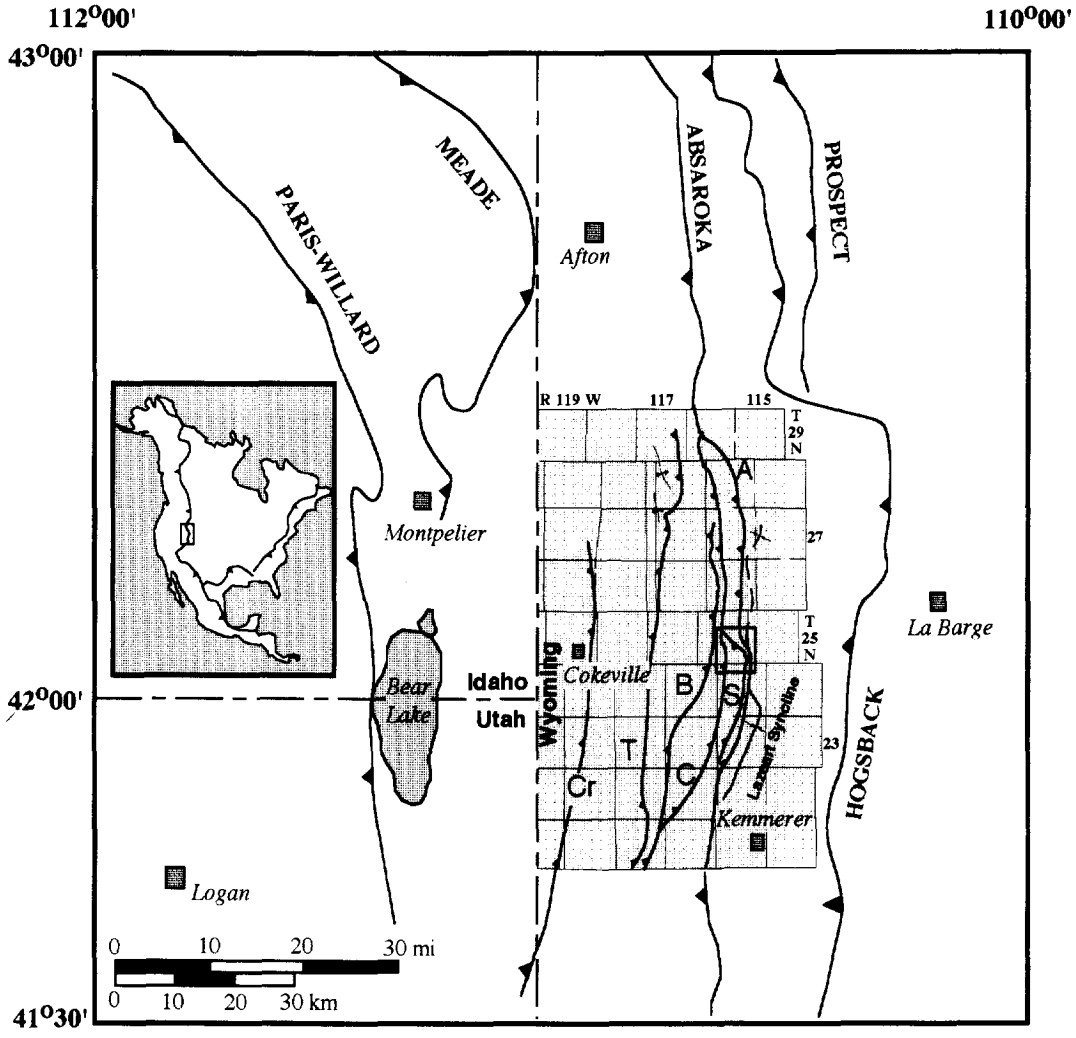

Fig. 2. Location map of the central part of the thrust belt. Major thrust sheets are: the Paris-Willard, Meade, Crawford (Cr), Absaroka (A), Hogsback. Fine grid lines give township (T) and range (R) reference numbers. Shaded inset shows structural framework of the northern Fossil Basin, and study area within T25N, R116W. Thrusts associated with the Absaroka system also include the Tunp (T), Beaver Creek (B), Commissary (C), and the South Fork (S).

portion of the South Fork thrust is conservatively described as steeply-dipping.

Restored cross-sections

Two locally restored dip sections and one strike section constrain the geometry and minimum displacement along the South Fork thrust. The restored state versions of these sections are found in Apotria (1990) and are both admissible and viable (Marshak & Mitra 1988). Bedding thicknesses were determined from outcrop where possible, and otherwise from the literature (e.g. Oriel & Platt 1980, Lamerson 1982). Lamerson's (1982) cross-sections provide subsurface control based on seismic and well data, including thicknesses and a structure contour map on top of the Absaroka fault plane.

Section A–A′ (Fig. 4a) and section B–B′ (Fig. 4b) are positioned parallel to the inferred transport direction to the north and south of the oblique ramp. Strike section C–C′ (Fig. 4c) was drawn approximately parallel to the trace of the Absaroka thrust, intersecting the South Fork thrust.

Measured minimum displacements across the South Fork thrust are on the order of 290 m in A–A′, compared to about 166 m in B–B′ indicating differential displacement along strike of the South Fork thrust. The projected depth to the Absaroka thrust is 483 m deeper along section C–C′ to the south (A–A′) than to the north (B–B′). Honoring the surface geometry and projecting beds down to the level of the detachment within the Ordovician Bighorn dolomite indicates substantial relief on the Absaroka thrust plane. The perturbation is visible on a structure map of the Absaroka thrust plane based on well and seismic data (fig. 23 of Lamerson 1982), and is also marked by a change in stratigraphic separation of the Absaroka thrust near the South Fork oblique ramp.

MESOSCOPIC STRUCTURES

The geometry of the oblique ramp and the orientation of associated fabric elements suggested the study area be divided into three structural domains: (a) the region to the north of the oblique ramp comprising its footwall, (b) the region in the hangingwall directly above the

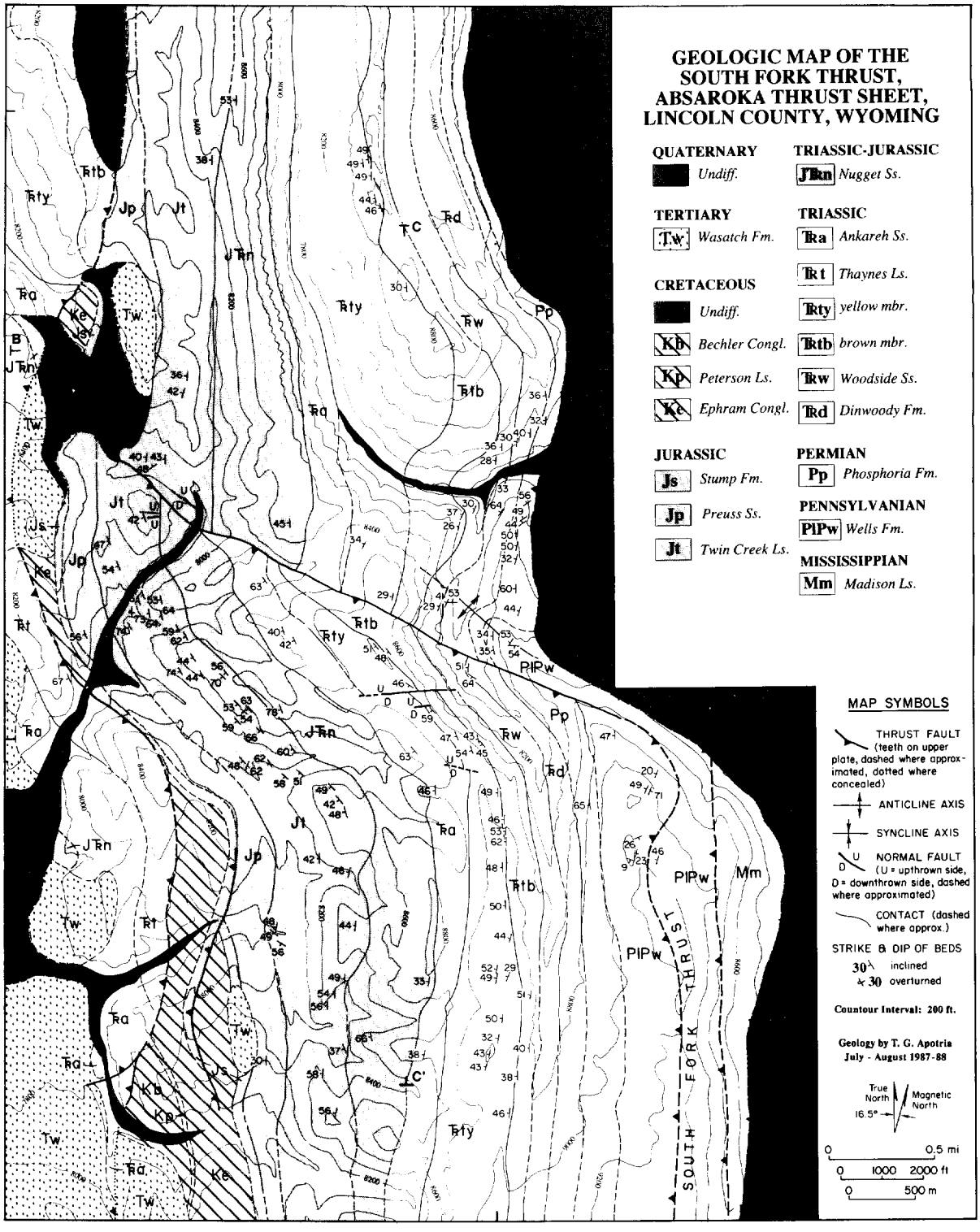

Fig. 3. Geologic map of the study area (originally mapped at 1:12,000). Dip section lines A–A′, B–B′, and strike section C–C′ are featured in Fig. 4.

oblique ramp where bedding strikes N30°W, and (c) the region to the south of the oblique ramp where bedding strikes N0°E.

Folds

Fold were documented in both the hangingwall and footwall of the South Fork oblique ramp (Fig. 5). The folds are outcrop scale, with amplitudes ranging from less than one meter to several meters. Several folds exhibit significant westward plunge.

Folds are separated into three groups on the basis of location and orientation. Group 1 folds trend subparallel to local bedding strike, are located away from the trace of the oblique ramp, and generally indicate E- to SE-directed shortening (folds **a–g**, Fig. 5).

Group 2 folds lie in the hangingwall and footwall of the South Fork thrust near the frontal ramp–oblique ramp intersection (**k–o**). These fold trends in the

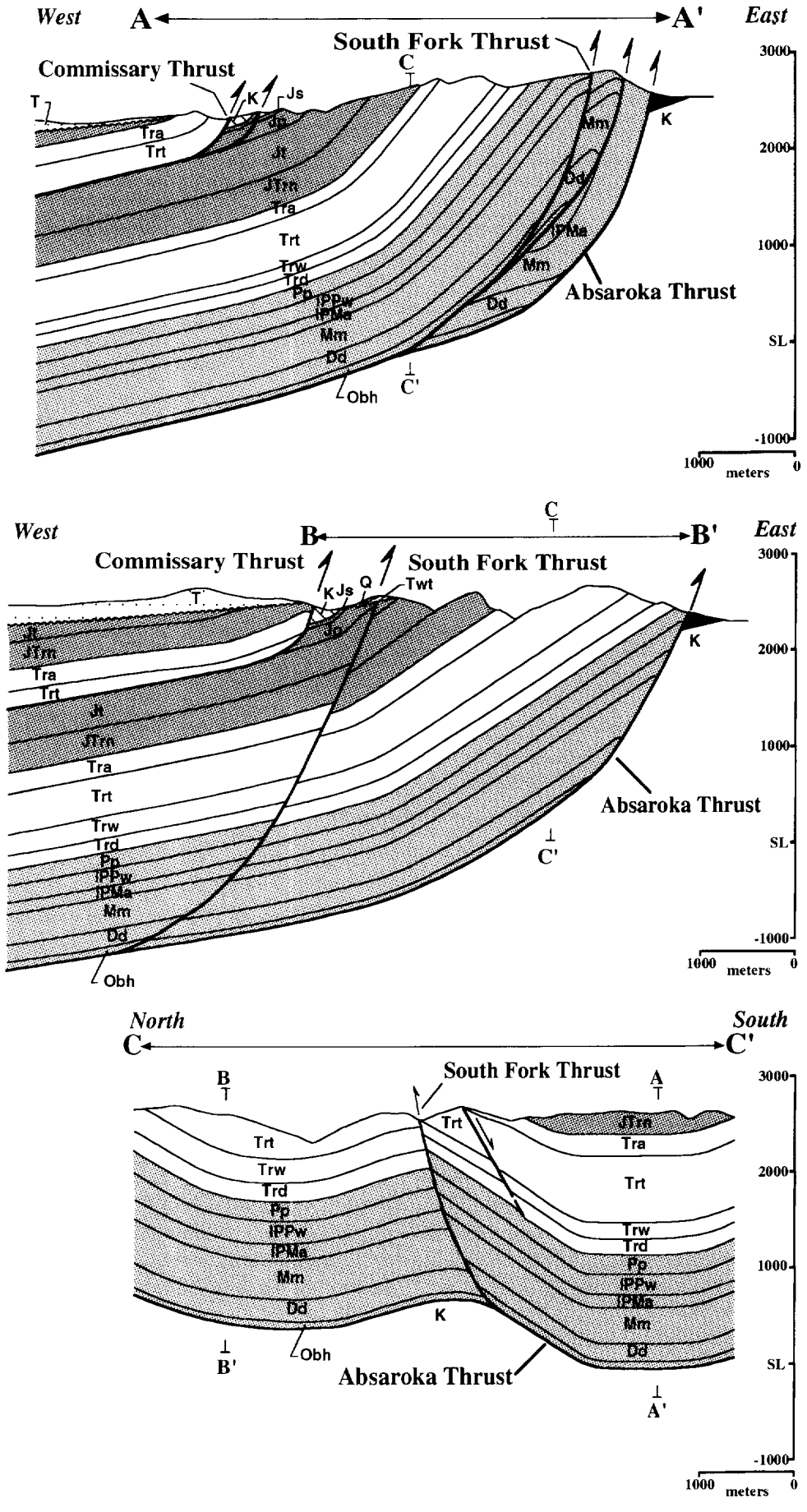

Fig. 4. Strike and dip vertical cross-sections. Thicknesses are assumed constant within sections A–A′ and B–B′. Section locations are indicated on the map in Fig. 3. Arrows indicate the extent of the cross-sections on the map in Fig. 3. No vertical exaggeration.

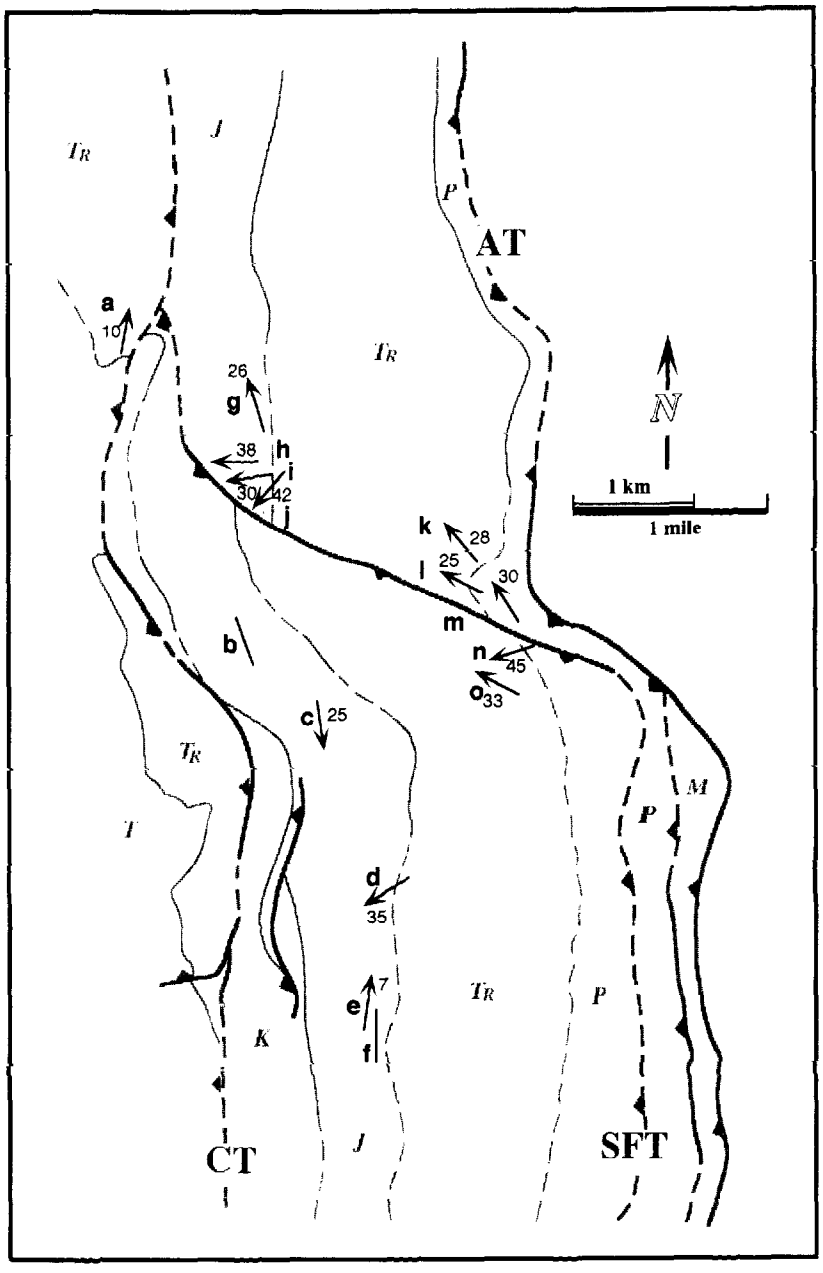

Fig. 5. Generalized geology and fold location map. Arrows indicate the trend and plunge of fold axes. Bold symbols indicate fold labels referred to in the text. AT = Absaroka Thrust, SFT = South Fork Thrust, CT = Commissary Thrust.

hangingwall and footwall are not parallel to bedding strike, but at a low angle to the trace of the South Fork thrust.

Group 3 folds are located in the footwall near the western terminus of the South Fork ramp (**h, i, j**). Axes are notably different than those in Groups 1 and 2, and have azimuths ranging from N45E (**j**) to N90E (**h**), generally indicating N- to NW-directed shortening.

Fractures

The attitude of some 1300 systematic fractures were measured in the Jurassic Twin Creek Formation (700) and Triassic Thaynes Formation (600). In the Twin Creek limestone, measurements were restricted to the Watton Canyon Member, a massive, oolitic, well-exposed ridge-former (Imlay 1967). Many fracture planes (sets 2 and 3 below) were pitted by pressure solution cleavage, thus obscuring consistent observations of fracture surface morphology and timing. No fracture planes exhibit measurable shear offset, and most were not mineralized. Each fracture set is nearly perpendicular to bedding.

The strike of dominant fracture sets for each station are plotted in plan view (Fig. 6). Three systematic fracture sets are most common at each station. The most complete representation of fracture distribution comes from the Thaynes Limestone in the southern domain (TyS, Fig. 6). Set 1 strikes ~N90°E, set 2 strikes ~N22°E and set 3 strikes ~N39°W. The variation in other domains is stronger, and some fractures are not well represented. Fracture set 1 generally strikes perpendicular to the strike of bedding. North and south of the oblique ramp, set 1 fractures are sub-perpendicular to

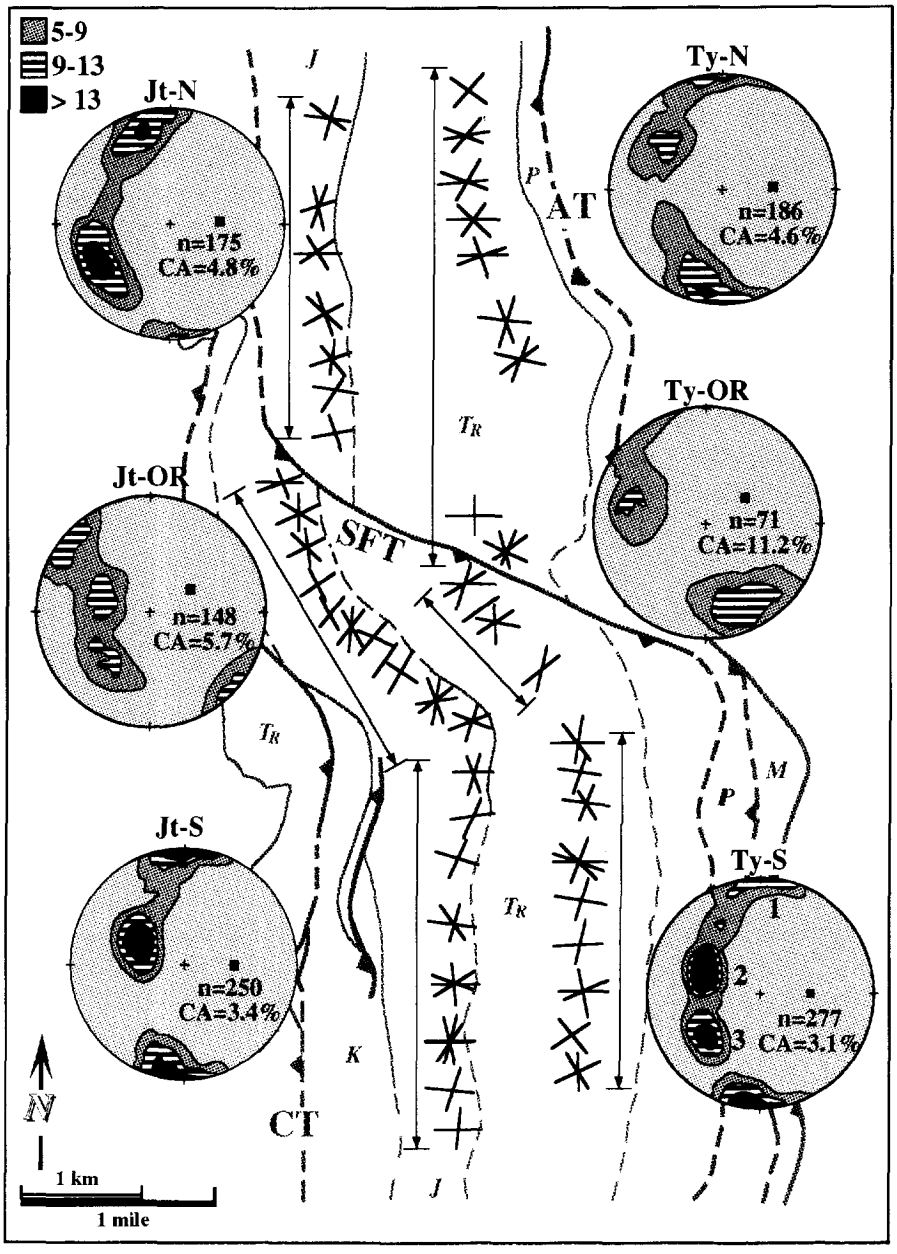

Fig. 6. Fracture azimuth map in the Twin Creek (west) and Thaynes (east) limestone. At each station, azimuths of the most dominant fracture sets are shown. Kamb (1959) contours of poles to fracture planes in the Thaynes (Ty) and Twin Creek (Jt) are plotted in the structural domains north (N), and south (S) of the oblique ramp (OR). Equal-area, lower-hemisphere projections with the plane of projection horizontal. The mean pole to bedding is indicated by the solid square. **n** is the number of contoured measurements, **CA** represents the percentage of the area of the stereonet used as a counting area. Contour intervals represent standard deviations starting with 5 with the intervals shown.

the regional trend of the Absaroka thrust (cross-strike fractures). Fracture sets 2 and 3 are apparent conjugates and are often acutely or obtusely bisected by the strike of bedding.

Fractures over the oblique ramp consistently change orientation with respect to similar sets to the north and south. Over the oblique ramp, set 1 fractures are oriented 30–40° counterclockwise with respect to those found north and south of the oblique ramp. A similar rotation is observed for sets 2 and 3. If fractures had formed prior to displacement along the South Fork thrust, they can be used as passive markers. Otherwise, they may have formed during or after South Fork thrust movement.

A model for the origin and timing of the fractures at the South Fork oblique ramp should account for the following observations: (1) two to three systematic fracture sets are common to each region, (2) the fractures appear to maintain a consistent orientation subperpendicular to bedding, (3) a systematic change in the attitude of bedding and fractures is observed above the oblique ramp proper with respect to domains to the north and south, (4) no fracture sets are unique to the oblique ramp.

With respect to the structural domains to the north and south, bedding above the oblique ramp is rotated some 30° counterclockwise due to differential displacement of the South Fork thrust. To test the hypothesis that the fractures were passively rotated, best-fit poles to fractures from Fig. 6 (Ty–S) are rotated 30° (counter-

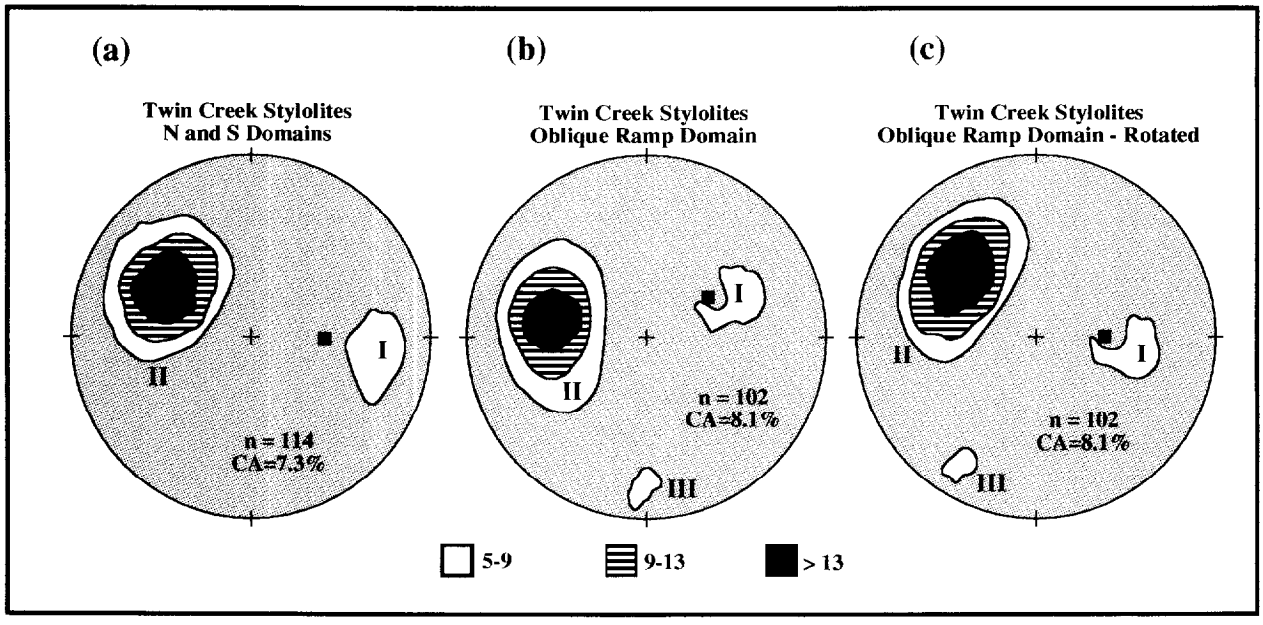

Fig. 7. Kamb contours of poles to tectonic stylolitic cleavage planes in the Twin Creek Formation. Two tectonic cleavage sets are indicated by Roman numbers II, III. The mean pole to bedding is indicated by the solid square. Kamb (1959) contour intervals represent standard deviations starting with 5. (a) Cleavage sets in structural domains north and south of the oblique ramp. (b) cleavage sets above the oblique ramp. (c) cleavage data from (b) rotated 30° counterclockwise about a vertical axis and contoured.

clockwise in map view) about a vertical axis. The resulting best-fit poles are consistent with those observed over the oblique ramp, particularly fracture set 1 (Jt–OR, Ty–OR, Fig. 6). Other rotation schemes were tested (e.g. rotation about an axis parallel to the strike of the oblique ramp) with results inconsistent with the data.

Stylolitic cleavage

Stylolitic cleavage planes were measured from the Jurassic Twin Creek Formation, in the light grey, medium–coarse grained Leeds Creek Member, stratigraphically below the Watton Canyon member (Imlay 1967). The same structural domains used for fracture analysis were used to analyze the cleavage data. In all but a few cases, stylolitic 'teeth' are perpendicular to the cleavage plane. The poles to stylolitic cleavage planes indicate the direction of principal shortening strain at the time of their formation (Sorby 1908, Fletcher & Pollard 1981). Unambiguous timing relationships between stylolite sets were absent.

Set I and II stylolites are common to all domains, and set III is unique to the oblique ramp (Fig. 7). Set I stylolites are consistently oriented subparallel to bedding. These are likely due to compaction strain and are not discussed further. Set II represents the bulk of the measurements recorded, due to their common exposure sub-parallel to systematic fracture set 2. In the case where the wavy stylolite and fracture plane intersects at a low angle, an irregular closed stylolite surface appears on the face of the fracture plane. In the north and south domains, the set II poles have a mean attitude of 32°, N60°W (Fig. 7a). Above the oblique ramp, the mean attitude is 35°, N83°W (Fig. 7b). Set II stylolites are nearly perpendicular to bedding. The expected regional shortening direction is west to east, yet the shortening direction inferred from stylolites of the north and south domains is east–southeast.

Set III stylolites are unique to the hangingwall above the oblique ramp, and have a mean pole with an attitude of 12°, S2°W (Fig. 7b). With rare exception, the teeth are perpendicular to the stylolite plane. Set III stylolite cleavage planes are subparallel to set 3 fracture planes.

Discussion of stylolite data

The observations described above suggest that sets II and III stylolites may have formed on pre-existing fracture planes or alternatively, fractures opened along pre-existing stylolites. North and south of the oblique ramp, set III stylolites are absent, yet set 3 fractures are present. This suggests that stylolite set III formed on set 3 fractures locally due to stresses associated with the oblique ramp. Rather than pressure solve on a new plane perpendicular to the maximum shortening strain, pressure solution may have preferentially occurred on pre-existing fractures where fluid flow was probably enhanced (Geiser & Sansone 1981). Srivastava & Engelder (1990) documented stylolites that formed on the face of open fractures in the Valley and Ridge province of Pennsylvania. They suggest that outer arc extensional bending stresses at the lower hinge of a fault-bend fold propagate strike-parallel fractures. As these rocks move up the ramp and pass through the upper hinge of the fault-bend, inner-arc compressional bending stresses stylolitized the pre-existing fractures. Simi-

Table 1. Calcite twin orientation data and strain derived from the Groshong (1972) technique. CP = cleaning procedure where ALL = all twins from sample, PEV = positive expected values only, NEV = negative expected values only. LDR = 20% of largest magnitude deviations removed. E1, E2 and E3 are the maximum, intermediate and minimum principal strains where contraction is negative. $\sqrt{J2}$ is the second invariant of deviatoric strain, a measure of the total distortion by twinning measured in percent strain

		Twin sets		Principal strains			Strain orientation					
Sample	Bedding	CP	#	E1	E2	E3	E1	E2	E3	NEVs(%)	Intensity (#/mm)	$\sqrt{J2}$
Ty-16	012/44W	ALL	111	−0.5	0.15	0.352	304/26	96/61	209/12	24	25.9	0.45
		PEV	84	−0.742	0.161	0.581	302/31	114/58	209/3	2.4	26.1	0.68
		NEV	27	−0.64	−0.19	0.82	212/2	119/64	303/26	7.4	25.2	0.75
		LDR	89	−0.55	0.16	0.39	307/22	60/44	200/38	18	22.5	0.49
Ty-74	000/49W	ALL	111	−0.83	0.09	0.93	246/40	349/15	95/46	15.3	47.5	0.87
		PEV	94	−0.82	−0.33	1.15	230/40	337/20	87/43	1.1	49.9	1.03
		NEV	17	−1.42	−0.08	1.51	80/42	294/42	187/18	11.8	33.5	1.47
		LDR	89	−0.87	−0.2	1.06	222/36	330/24	87/44	9	44.6	0.98
Ty-81	006/54W	ALL	91	−0.27	−0.1	0.38	81/27	211/51	337/25	36.3	30.2	0.34
		PEV	58	−1.14	−0.12	0.67	91/33	236/52	349/17	5.2	32.7	0.84
		NEV	33	−0.79	0.12	1.26	322/39	167/48	63/13	0	25.8	0.97
		LDR	73	−0.45	−0.16	0.61	76/16	184/48	334/38	30.1	27	0.55
Ty-84	342/39SW	ALL	116	−0.78	0.13	0.65	198/13	99/34	305/53	32.8	36.8	0.72
		PEV	78	−1.24	−0.05	1.29	201/12	100/42	303/46	6.4	40.1	1.27
		NEV	38	−0.93	0.22	0.72	295/41	69/39	181/25	10.5	30.4	0.85
		LDR	93	−1.2	0.23	0.98	199/10	100/41	299/47	21.5	34.3	1.11
Ty-86	337/49SW	ALL	136	−0.32	−0.13	0.44	259/24	352/6	95/66	29.4	23.8	0.40
		PEV	96	−0.48	−0.16	0.64	259/25	353/10	103/63	2.1	25.7	0.58
		NEV	40	−0.52	0.13	0.38	124/61	336/26	239/14	15	19.3	0.46
		LDR	109	−0.41	−0.16	0.57	248/21	341/8	91/68	19.3	21.4	0.51
Ty-88	328/49SW	ALL	112	−0.42	−0.07	0.49	172/6	264/17	65/72	46	3.92	0.46
		PEV	61	−1.1	−0.23	1.29	347/2	256/17	84/73	0	44.2	1.21
		NEV	51	−1.26	0.14	1.12	86/71	262/19	353/1	11.8	33.4	1.20
		LDR	90	−0.45	0.003	0.44	117/0	267/24	87/66	45.6	34	0.45
Ty-89	010/29NW	ALL	94	−0.72	−0.1	0.82	195/13	289/14	65/71	27.7	40.2	0.77
		PEV	68	−1.16	−0.18	1.34	196/13	290/13	62/71	0	43.5	1.26
		NEV	26	−1	0.31	0.69	62/57	289/23	190/21	3.8	31.4	0.89
		LDR	75	−0.67	−0.06	0.73	197/15	292/19	70/66	30.7	35.4	0.70
Ty-90	027/34NW	ALL	110	−0.59	0.14	0.45	81/8	340/54	177/35	29.1	40.1	0.53
		PEV	78	−1.2	0.06	1.09	83/10	333/63	178/25	5.1	41	1.15
		NEV	32	−1.06	−0.12	1.18	177/10	301/73	84/14	12.5	37.7	1.12
		LDR	88	−0.55	0.16	0.4	76/12	316/66	170/20	25	34.7	0.49

lar observations were documented by Dean *et al.* (1988) in southeastern West Virginia.

To test the timing of stylolitization in a way similar to that previously tested for fractures, poles to set II and III stylolite planes over the oblique ramp are rotated 30° clockwise about a vertical axis (Fig. 7c). As a result, there is virtually no statistical difference in orientation of stylolite set II between all three domains. In addition, the mean pole to set III stylolites is oriented 10°, S30°W after this rotation is removed. This orientation suggests the inferred principal shortening direction is at a high angle to the strike of the oblique ramp.

MICROSCOPIC STRUCTURES: CALCITE TWINNING STRAIN

The strain by calcite twinning is measured using the strain-gauge technique (Groshong 1972, 1974). Eight samples were collected from the upper yellow–grey member of the Triassic Thaynes Formation and twins were measured from 2 to 3 orthogonal thin sections. Of the eight samples analyzed, samples Ty-74 and Ty-16 were collected to the north and south of the South Fork oblique ramp (bedding: ~N0°E/40°W) in order to estimate the 'regional' or far-field deformation. Other samples were collected in the hangingwall and footwall of the oblique ramp. Groshong (1974) has suggested two noise reduction techniques be applied to the entire data set (ALL). The first involves removing 20% of the largest magnitude deviations to eliminate grains with the most inhomogeneous strains and the largest measurement errors (LDR). In the second procedure, the positive (PEV) and negative (NEV) expected values are computed separately. A negative expected value suggests a negative sense of shear for a given twin set (e.g. a grain that should not have twinned given the calculated strain tensor). Groshong (1972) suggested that a large number of negative expected values with large strains might indicate inhomogeneous strains or superposed homogeneous strains.

Strain gauge results

The least-squares strain results are summarized in Table 1. Equal-area, lower-hemisphere projections of the strain from the positive expected values are plotted

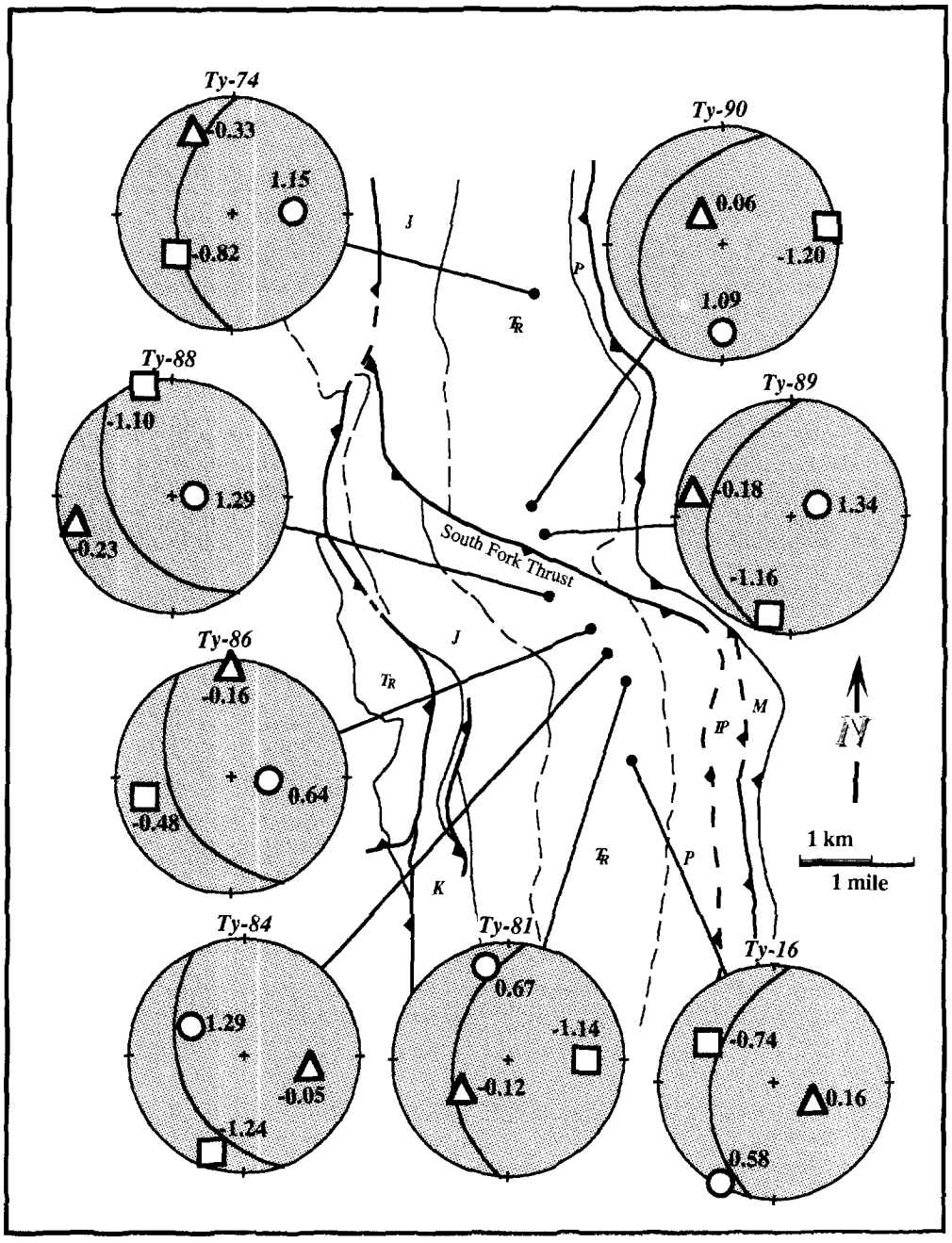

Fig. 8. Map indicating Thaynes Formation sample localities for calcite strain analysis. Stereoplots of least squares strain axes derived from calcite strain gauge technique. Lower hemisphere, equal area projections of the maximum (square), intermediate (triangle), and minimum (circle) principal strains. Magnitudes are indicated beside each axis where shortening is negative. The orientation of bedding is indicated by the great circle.

on a generalized map of the study area (Fig. 8). Principal shortening strain magnitudes for all data sets are less than 1.5%. In general, those samples closest to the oblique ramp have the highest strain magnitudes and the largest percentage of NEVs. The PEV data indicate an increase in strain magnitude relative to ALL, PEV and NEV, but no significant change in orientation. NEVs, when tested separately, indicate an axis flip between the maximum (E1) and minimum (E3) strain relative to ALL, PEV and LDR populations. In samples where the principal shortening strain is at a high angle to bedding, the strain gauge technique may record early compaction strains in the NEV population. However, as pointed out by Burkhard (1993), the interpretation of multiphase deformation from NEV strain axes which are orthogonal to PEV axes is suspect.

Previous work documenting calcite strains within fold and thrust belts suggest that twinning occurs early in the deformation history. In host rock calcite, the maximum shortening direction and compression axis, are in most cases parallel to bedding and the transport direction in folds, (Friedman & Stearns 1971, Chapple & Spang 1974, Groshong 1974), and in thrust sheets (Spang & Brown 1981, Spang *et al.* 1981, Wiltschko *et al.* 1985, Craddock *et al.* 1988, Kilsdonk & Wiltschko 1988).

Samples Ty-16, Ty-74 exhibit E1 sub-parallel to bedding and the regional transport direction, typical of the early stages of layer-parallel shortening. Strain magni-

tudes and NEVs are generally the lowest among the eight samples. The slight deviation from east–west shortening by E1 is consistent with shortening directions inferred from set II stylolites within the Twin Creek Formation.

Hangingwall oblique ramp samples Ty-88, Ty-86, Ty-84 each record different components of deformation. Sample Ty-86 deformed similar to 'far-field' samples to the north and south. E1 trends N113°E, similar to sample Ty-16, when bedding is rotated back to regional strike about a vertical axis. Samples Ty-84 and Ty-88 both have high strain magnitudes, high percentage of NEVs and principal shortening directions oblique to bedding. E1 axes imply a N–NE-shortening direction at a high angle to the strike of the oblique ramp, when bedding strike is rotated back to regional. This direction is consistent with that inferred from Group 2 folds (Fig. 5) and set III stylolites (Fig. 7).

Sample Ty-81 is characterized by high strain magnitudes, high percentage of NEVs, E1 direction which is perpendicular to bedding. These orientations are not readily attributed to 'far-field' strains, or N–NE-directed shortening. The E1 direction could be attributed to early compaction or thrust ramping, both will impose vertical shortening strains in the overriding hangingwall (e.g. Kilsdonk & Wiltschko 1988).

The footwall adjacent to the South Fork oblique ramp shows evidence of folding (Fig. 5). Sample Ty-89 exhibits high strain magnitudes and NEVs with E1 axes sub-parallel to bedding strike. The direction of the E1 axis is N6°E when bedding is rotated back to regional strike. Sample Ty-90, approximately 325 m north of Ty-89, suggests E-directed shortening in the sample's current orientation, and N60°E directed E1 axes if bedding is rotated back to regional strike. This places the principal shortening direction at a high angle to the strike of the oblique ramp, similar to samples Ty-84, Ty-88, Ty-89.

The correlation between NEVs, the second invariant of strain ($\sqrt{J2}$) and distance from the ramp can be explained by either: (a) higher stresses near the oblique ramp which activate diversely oriented twins, (b) an increase in rotational or overprinted strain near the oblique ramp, and (c) an increase in the effects of inhomogeneous strains (e.g. twinning induced by fractures) near the oblique ramp. This correlation could occur if the greatest percentage of measured twins in a given sample corresponds to the 'regional' deformation, yet the twins with the highest strain magnitudes correspond to those associated with oblique ramp deformation. In general, the set of twin lamellae in each grain that becomes best developed (and emerges as E1 in the Groshong technique) is the set that is oriented most favorably to the load axis corresponding to the greatest magnitude of shortening (e.g. Friedman & Stearns 1971). If the penetrative strains were rotational, the spectrum of incremental strains are probably not decipherable from the Groshong technique, but are likely masked by the highest strain magnitude increment. Other mesoscopic data presented earlier support both (a) and (b), but cannot distinguish between the two. No evidence for case (c) was found. Craddock *et al.* (1988) observed that calcite is passively rotated with no effects of superposed strain; this is not consistent with the high NEV and $\sqrt{J2}$ values observed near the South Fork oblique ramp. Here, rotation of samples back to regional strike results in E1 axes which deviate from 'far field' shortening, suggesting that early calcite twins reflect superposed deformation prior to rotation.

INSIGHTS FROM MODELLING STUDIES

Recent modelling studies provide insight into the expected modes of deformation near oblique ramps. First, a kinematic model is used to understand three-dimensional particle paths over an oblique ramp, and the resultant out-of-plane strain that occurs at ramp intersections. Second, a mechanical model is described which predicts the principal stress directions and material velocities in the hangingwall moving over an oblique ramp. These results of both modelling approaches are compared to field data described earlier.

Kinematic models for the deformation of a hangingwall moving over an oblique footwall ramp were developed for two end-members of assumed macroscopic deformation mechanisms: vertical shear and layer-parallel shear (Apotria *et al.* 1992). For the case where the hangingwall deforms by layer-parallel shear, material particle paths are deflected out of the transport plane over an oblique ramp (Fig. 9a). The deflection and out-of-plane shear strains are zero for the special cases of pure frontal and lateral ramps, and maximum at an intermediate oblique orientation that depends on oblique ramp dip. At the trailing intersection zone which is concave toward the transport direction, divergence of hangingwall material results in lateral extension, or the development of a 'gap'. Similar deflection of the hangingwall was noted by Wilkerson *et al.* (1992) in tomographic analyses of sandbox models, in which sand layers with imbedded transport-parallel marker lines were shortened over rigid footwall templates similar to that in Fig. 9. In general, the predicted extension may be a mechanism for hangingwall tear faulting (oblique-slip normal faulting) or enhanced fracturing. At the leading intersection zone, which is convex toward the transport direction, displacement paths converge in the hangingwall resulting to lateral shortening, or 'overlap' (Fig. 9a). Ramp intersections should therefore be the locus of anomalous deformation in the hangingwall and indicate that layer-parallel shear alone cannot accommodate the deformation (Fig. 10). If the footwall deforms in a similar manner, out-of-plane deflection of the footwall produces lateral shortening at the trailing intersection and lateral extension at the leading ramp intersection (Fig. 9b). Observations made in the field are consistent with the model predictions (i.e. folds **h–j**, Fig. 5, hangingwall normal faults at the trailing oblique ramp–frontal ramp intersection). The layer-parallel shear model provides insight into the types of strain expected

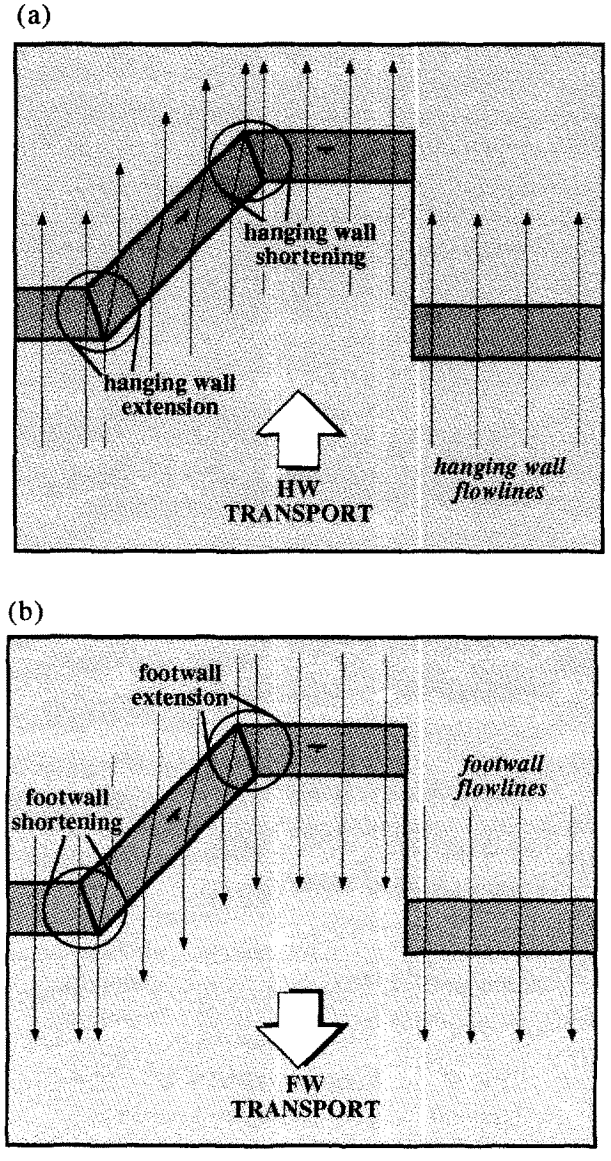

Fig. 9. Flat–ramp–flat geometry with modelled material flow lines. (a) Hangingwall flow over frontal ramp–oblique ramp intersections produces local shortening or extension. (b) Footwall flow over the same intersections produces the opposite sense of out-of-plane strains (from Apotria *et al.* 1992).

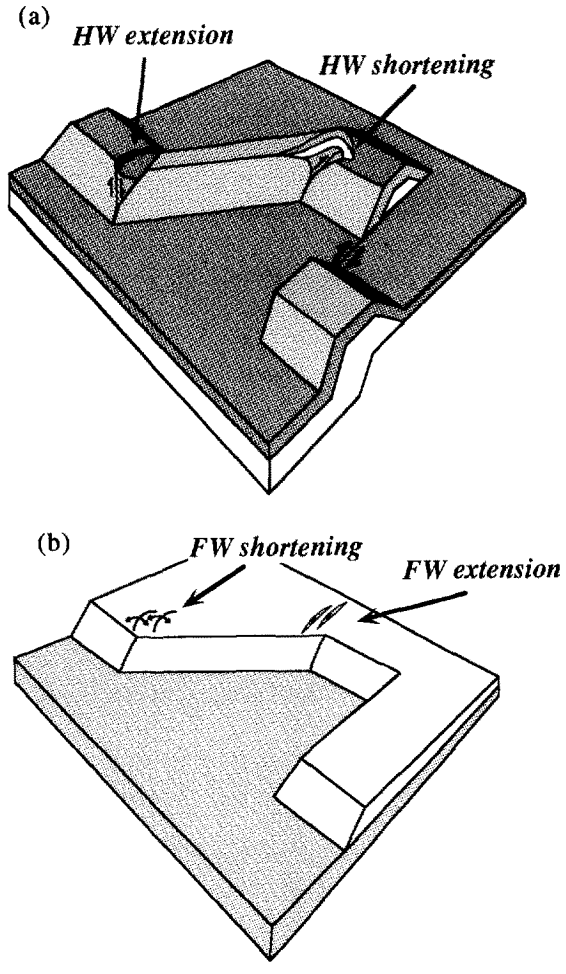

Fig. 10. Footwall geometry indicating the effects of three-dimensional deformation predicted from kinematic models. Out-of-plane flow produces local extension or shortening at ramp intersections in the footwall and hangingwall. Extension can be manifest as normal faults (tear faults) or enhanced fracturing. Shortening may result in reverse faults and folds at a high angle to the regional trend.

at ramp intersections, but does not explicitly address stress and strain magnitudes and orientations above the central region of the oblique ramp.

Apotria (1988, 1990) developed mechanical models based on the solution of a 3D continuum mechanics boundary value problem that provide further insight into the stresses above an oblique ramp. One model treats an oblique ramp as low-dip sinusoidal surface above which a linear viscous hangingwall (half-space) translates at a given velocity. The frictionless interface (detachment) induces a perturbed velocity and stress field which distorts the hangingwall (Fig. 11a). The distortion is a function of the local slope of the footwall and the height above the interface, with no far-field shortening or extension boundary conditions imposed. The model geometry is constant in the y-direction, and therefore does not address the complexities that occur at frontal ramp-oblique ramp intersections. The total velocity field is the sum of the perturbed velocity (due to distortion above the interface) and the translational velocity component. The hangingwall translates at an oblique angle (α) to the strike of the axis of the cylindrical ramp. The boundary value problem provides an analytical solution for the stresses, strain rates, and velocities in the upper half-space (hangingwall). The most significant result is that the maximum principal stress and strain rates occur in a plane perpendicular to oblique ramp strike, regardless of the angle between the strike of the ramp and the transport direction (α). The magnitude of the maximum principal stress and strain rate is maximum for $\alpha = 0°$ (frontal ramp) and a minimum for $\alpha = 90°$ (lateral ramp).

Stress deflections of this type have been observed elsewhere. For example, Casas *et al.* (1992) made similar observations near a lateral ramp in the Cameros thrust front, NW Iberian chain, Spain, and in finite element models. Casas *et al.* (1992) found that the principal compressive stress (σ_1) is deflected away from the transport direction, towards the normal to oblique ramp strike, similar to the analytic solution above.

To summarize, modelling results indicate that

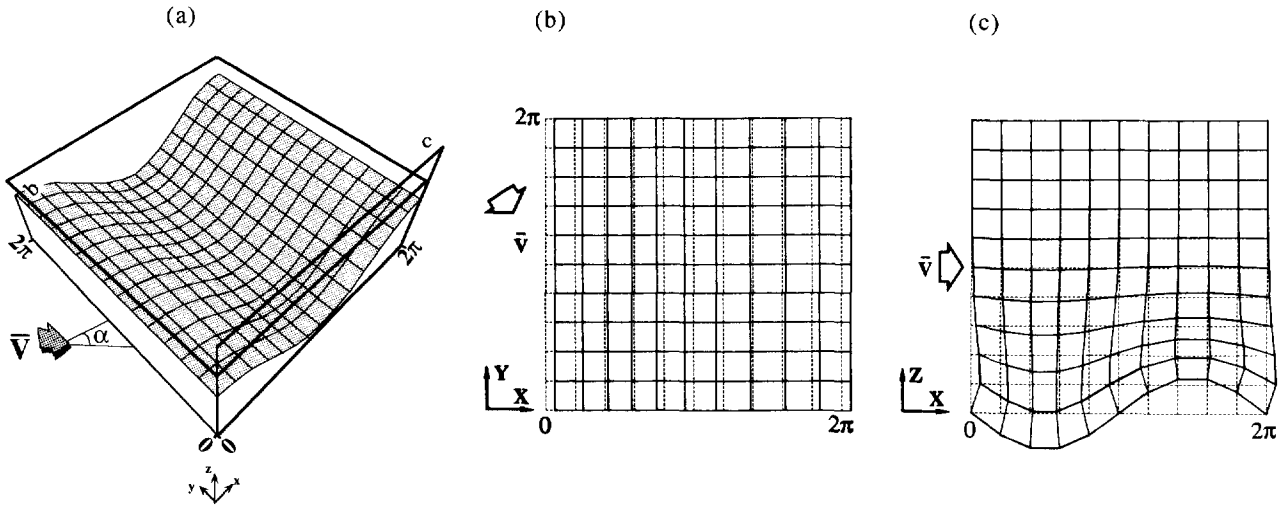

Fig. 11. (a) Cylindrical sliding surface represented by a sinusoid in the x-direction generated about the y-axis representing a detachment which is oblique to the transport direction (from Apotria 1990). The arrow indicates the direction of the basic flow ($\bar{V}$) of the viscous upper half-space (hangingwall), and varies from dip slip ($\alpha = 0°$) to strike slip ($\alpha = 90°$). (b) Deformed grid in the horizontal plane at a height above the interface of $L/2\pi$ where L is one wavelength in the x-direction. The solution shown is for the case where $\alpha = 60°$. The principal strain rates are always in the xz-plane, and are of greatest magnitude for the case of frontal ramps ($\alpha = 90°$) and least for lateral ramps ($\alpha = 0°$). (c) Deformed grid in the xz-plane suggesting that vertical shortening and horizontal extension occur above the normal fault ramp whereas vertical shortening and horizontal extension occur above the thrust fault ramp. Maximum deformation occurs at height $L/2\pi$ and becomes negligible at a height corresponding to about 0.5 the wavelength of the perturbation.

material points in the hangingwall are deflected away from the true dip of the oblique ramp (Fig. 9) and principal stresses and strain rates are in a plane perpendicular to the strike of the oblique ramp (Fig. 11). These model predictions are consistent with the observed orientation of folds, cleavage and calcite twinning strains in the hangingwall of the South Fork oblique ramp.

None of the models described above incorporate a boundary condition that includes rotation or footwall deformation. Field evidence suggests that these are important components to the kinematics of the South Fork thrust. The models therefore represent a simplification of the actual complex deformation near oblique ramps, yet provide a physical basis for interpreting many deformation mechanisms in the field.

INTERPRETATION AND DISCUSSION

Sources and timing of hangingwall rotation

The study area may have been affected by at least three sources of rotation: (a) rotation of the Absaroka hangingwall during ramping (~30°CCW rotation about a N-directed axis parallel to the strike of the Absaroka ramp), (b) rotation of the Absaroka hangingwall during ramping of the younger Hogback thrust to the east (~30° CCW rotation about a N-directed axis parallel to the strike of the Hogsback ramp), and (c) ~30° CCW rotation of the South Fork thrust hangingwall about a vertical axis. Cross-sections from this study (Fig. 4) and previous work (e.g. Lamerson 1982, Coogan 1992) indicate that the near-surface dip of the Absaroka thrust plane can be between 70° and vertical. The likely source of this steep dip is the rotation indicated in (b) above. The amount of rotation, however, is not well constrained. Lamerson (1982) indicates that the dip of the Hogsback footwall ramp is about 30° to the west, suggesting the same amount of rotation of the Absaroka sheet. However, some of the rotation above the Hogsback footwall ramp may have been accommodated by tightening of the Lazeart syncline (Delphia & Bombolakis 1988). The orientations of fractures and stylolitic cleavage are consistently subperpendicular to bedding, thus the interpretation of these data is not complicated by subsequent rotation due to Absaroka or Hogsback ramping. However, many of the folds documented in the study area show significant plunge (Fig. 5). The effects of either Absaroka or Hogsback ramping on fold orientations was tested by removing the rotation indicated in (b) above. This results in a reduction in the plunge of fold axes oblique to the regional trend, but not a significant change in fold trend. Therefore, such rotation does not significantly alter the inferred shortening directions.

The orientation of fractures, stylolitic cleavage, and deformed calcite twins above the oblique ramp relative to the same fabrics to the north and south, strongly suggest that rotation about a vertical axis was a significant component of the deformation. About 30° of counterclockwise rotation about a vertical axis best accounts for the change in attitude of these fabrics in the hangingwall. A group of small-offset normal faults mapped in the hangingwall near the center of the oblique ramp (Fig. 3) is consistent with the tangential extension that could occur during such rotation. As described previously, the sense of offset along the South Fork thrust varies from right lateral, to a point of zero apparent offset, to a left lateral offset near the leading oblique ramp–frontal ramp intersection. The hangingwall is con-

sistent with reverse offset at the western end (where the fault begins to change from SW- to W-dipping) and with strike-slip offset at the eastern end, relative to the footwall. The offset pattern indicates greater heave along the fault from west to east and is consistent with ~124 m more displacement to the south of the oblique ramp relative to the north (estimated in sections A–A′ and B–B′ in Fig. 4).

The argument can be made that the change in fracture orientation above the oblique ramp reflects fractures formed by deflected stress trajectories. However, fractures maintain a consistent orientation with respect to bedding above the oblique ramp, rather than with the strike of the fault. In addition, there does not appear to be a set of fractures unique to the oblique ramp. On these grounds, fractures are argued to have formed earlier than the 30° CCW rotation about a vertical axis.

Penetrative deformation adjacent to oblique ramp

Three groups of data suggest that the oblique ramp imposed a distinct deformation event on the hangingwall and footwall. Group 2 folds (**k–o**) have axes which are sub-parallel to the strike of the ramp. This suggests shortening which is NE-directed, sub-perpendicular to strike of the ramp. Group 3 folds (**h,i,j**) appear to be distinct in orientation from group 1 and 2 folds, and are related to the trailing frontal ramp–oblique ramp intersection (Fig. 9b).

Set III stylolitic cleavage is found in the hangingwall above the oblique ramp, and may have formed on pre-existing fractures. The principal shortening direction of set III is north–northeast based on the best-fit pole to contoured data (Fig. 7). Stylolite set II adjacent to the oblique ramp restores parallel to set II to the north and south when rotated 30° clockwise about a vertical axis. This suggests set II formed prior to rotation. The same rotation of stylolite set III places the inferred principal shortening direction nearly perpendicular to the strike of the oblique ramp.

Twinning strains measured in samples Ty-90, Ty-89, Ty-88, and Ty-84 adjacent to the oblique ramp record principal shortening strains which deviate significantly from transport and bedding parallel. When bedding attitude is restored to its regional orientation, these samples display shortening directions which are sub-perpendicular to the strike of the oblique ramp, consistent with group 2 folds, set III stylolites, and mechanical model results. These samples also have high NEVs and magnitudes, which supports the interpretation that they recorded a shortening strain at a high angle to the oblique ramp superposed on layer and transport-parallel shortening.

Summary of the kinematics of the South Fork oblique ramp

Both modelling approaches (kinematic and mechanical) have implicitly assumed frictionless sliding of the hangingwall over a rigid footwall. Field mapping suggests that the fault geometry and kinematics are more complex. The small displacement of the hangingwall and the high angle geometry of the oblique ramp suggest that the hangingwall did not simply slide from a lower footwall flat, up the oblique ramp, and onto the upper footwall flat, as the models idealize. Instead, footwall folding and thrust sheet rotation due to differential displacement are two fundamental components of the deformation.

Four stages of oblique ramp deformation are depicted schematically (Fig. 12). In stage one (Fig. 12a), a layer-parallel shortening fabric formed prior to or during early motion of the Absaroka thrust sheet (e.g. calcite twinning strains, group 1 folds). Strike-normal (cross-fold) fractures probably formed while the minimum stress was horizontal and normal to the maximum compression direction during thrusting. With continued thrusting and uplift, sets II and III fractures may have formed associated with outer-arc bending stresses at the lower hinge of the Absaroka ramp. Set II fractures acted as later pressure solution surfaces for set 2 stylolites which indicate shortening in an east–southeast direction, consistent with calcite twinning strain in sample Ty-16. In stage two (Fig. 12b), during emplacement of the Absaroka sheet to its final position, the South Fork thrust localized above a subthrust antiform visible on cross-section C–C′ (Fig. 4) and on Lamerson's (1982) structure map of the Absaroka thrust plane. In stage three (Fig. 12c), continued thrusting resulted in minor displacement along the South Fork thrust. The oblique ramp imposed NE-directed shortening strains, including calcite twinning, and set III stylolite cleavage which formed on set III fracture planes. Northeast-directed shortening also folded the footwall, as indicated by fold axes which are subparallel to the South Fork thrust trace (folds **k,l,m**, Fig. 5). Out-of-plane displacement near the trailing termination of the oblique ramp resulted in local lateral extension of the hangingwall and shortening of the footwall. In stage four (Fig. 12d), the oblique ramp portion of the South Fork thrust locked, with continued motion along the frontal ramp portion to the south resulting in a counterclockwise rotation of the hangingwall ~30° about a vertical axis. This last stage rotated all previous fractures and shortening fabrics as passive markers.

To summarize, certain components of the total strain at an oblique ramp are similar to those at frontal ramps, namely shortening in a plane at a high angle to the strike of the ramp. Differences result from deflection of hangingwall and footwall material out of the transport plane, resulting in convergence (lateral shortening) or divergence (lateral extension) at frontal ramp–oblique ramp intersections. Lateral extension may be one mechanism for the origin of tear faults, which in this case are interpreted to be normal faults with oblique slip. In general, if an oblique ramp is shallowly-dipping, the hangingwall may move from the lower flat, up the ramp, and onto the upper flat. If oblique ramp dip is steep as in the case of the South Fork oblique ramp, bending and sliding resistance which increase with ramp dip (e.g.

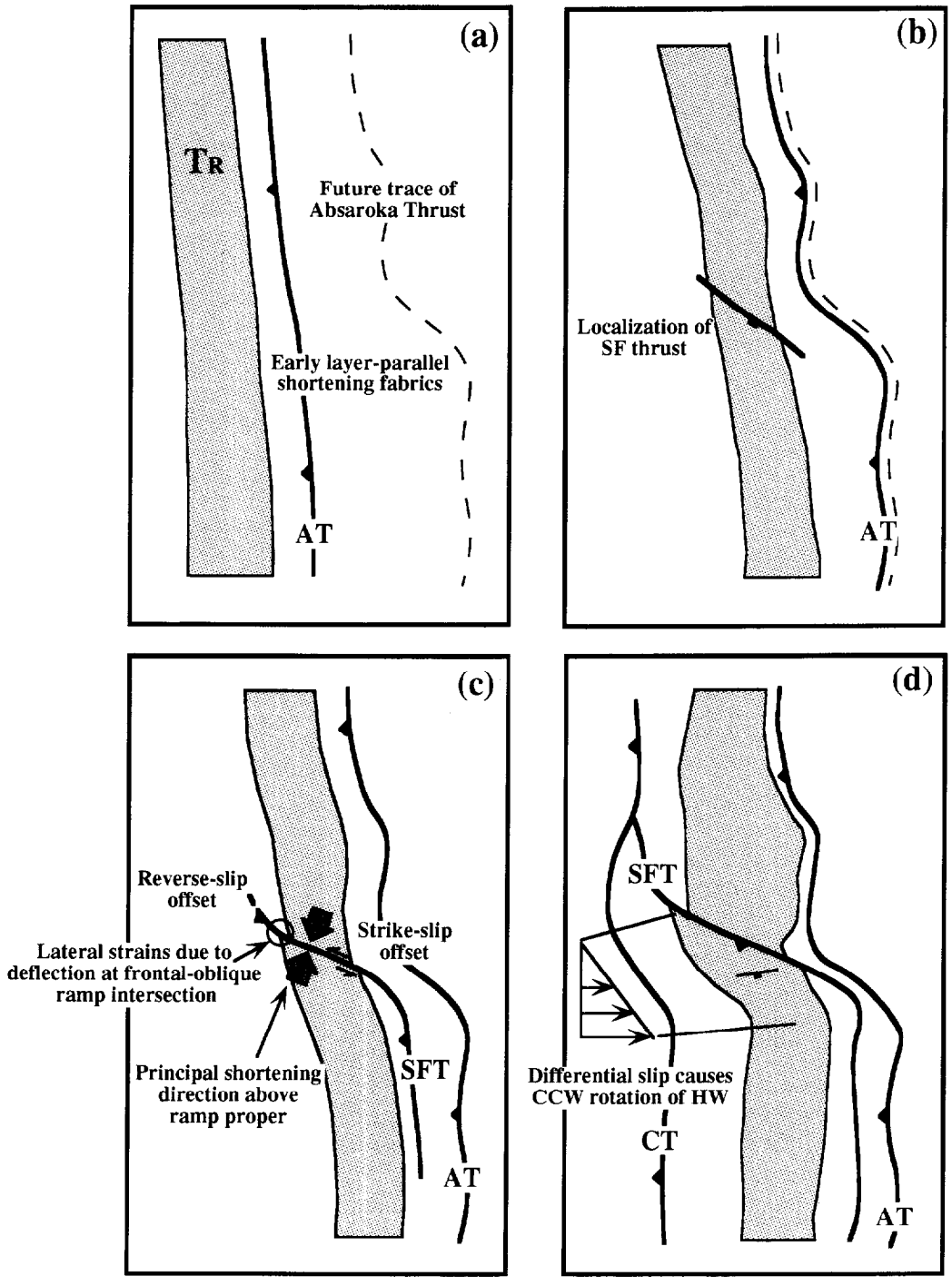

Fig. 12. Four stages of South Fork oblique ramp deformation. (a) Emplacement of Absaroka Thrust. (b) South Fork thrust is localized above a perturbation in the Absaroka thrust plane. (c) The South Fork thrust lengthens with displacement and causes penetrative deformation above the ramp. (d) Translation of the hangingwall is impeded by its steep dip, and rotates counterclockwise about a vertical axis. AT = Absaroka Thrust, TR = map trace of Triassic rocks, SFT = South Fork Thrust, CT = Commissary Thrust.

Wiltschko 1979) may impede displacement up the ramp inducing footwall deformation. Further differential transport causes thrust sheet rotation.

Acknowledgements—This paper represents partial fulfilment of a Ph.D. dissertation completed at the Center for Tectonophysics and Department of Geology at Texas A&M University. The critical comments and support of John Spang and David Wiltschko are gratefully acknowledged. This work also benefited from discussions with Mel Friedman, Brann Johnson, Raymond Fletcher and Peter Tauvers. JSG reviewers Steven Marshak, Mary Beth Gray and Steven Wojtal significantly improved the manuscript. Assistance during field mapping was provided by Douglas Goff and Paul Santi. Cathy Wall, LouAnn Beckman and Florence Rollens of Shell Development Company provided drafting assistance. Financial support was contributed by Sigma Xi, the Geological Society of America, and Texas A&M University. Generous industry support came from Texaco E&P Technology Division, ARCO Oil and Gas Co., Shell Western E&P Inc., Chevron U.S.A. Inc., Unocal Science and Technology Division, Conoco Inc. and Mobil Research and Development Corporation.

REFERENCES

Apotria, T. G. 1988. A 3-D solution for hangingwall motion over a wavy fault surface. *Geol. Soc. Am. Abstr. w Prog.* **20-7**, A57.

Apotria, T. G. 1990. The kinematics and mechanics of oblique ramp

deformation in fold and thrust belts, unpublished Ph.D. Dissertation, Texas A&M University, College Station, Texas.
Apotria, T. G., Snedden, W. T., Spang, J. H. & Wiltschko, D. V. 1992. Kinematic models of deformation at an oblique ramp. In: *Thrust Tectonics* (edited by McClay, K.). Chapman & Hall, 141–154.
Armstrong, R. L. & Oriel, S. S. 1965. Tectonic development of the Idaho–Wyoming thrust belt. *Bull. Am. Ass. Petrol. Geol.* **71**, 1847–1866.
Boyer, S. E. & Elliot, D. 1982. Thrust systems. *Bull. Am. Ass. Petrol. Geol.* **66**, 1196–1230.
Boyer, S. E. 1985. Hydrocarbon trap styles in fold and thrust belts and related terranes. Offshore Technology Conference. OTC 4873, 297–305.
Burkhard, M. 1993. Calcite twins, their geometry, appearance, significance and stress/strain markers and indicators of tectonic regime; a review. *J. Struct. Geol.* **15**, 351–368.
Butler, R. W. H. 1982. Hanging wall strain: a function of duplex shape and footwall topography. *Tectonophysics* **88**, 235–246.
Casas, A. M., Simon, J. L. & Seron, F. J. 1992. Stress deflection in a tectonic compression field: a model for Northwestern Iberian Chain, Spain. *J. geophys. Res.* **97-B5**, 7183–7192.
Chapple, W. M. & Spang, J. H. 1974. Significance of layer-parallel slip during folding of layered sedimentary rocks. *Bull. geol. Soc. Am.* **84**, 1523–1534.
Coogan, J. C. 1992. Thrust systems and displacement transfer in the Wyoming–Idaho–Utah thrust belt. Ph.D. dissertation, University of Wyoming.
Coward, M. P. & Kim, J. H. 1981. Strain within thrust sheets. In: *Thrust and Nappe Tectonics* (edited by McClay, K. & Price, N. J.), *Spec. Publ. geol. Soc. Lond.* **9**, 275–292.
Craddock, J. P., Kopania, A. A. & Wiltschko, D. V. 1988. Interaction between the northern Idaho–Wyoming thrust belt and bounding basement blocks, central western Wyoming. In: *Interaction of the Rocky Mountain Foreland and the Cordilleran Thrust Belt* (edited by Schmidt, C. J. & Perry, W. J.). *Mem. geol. Soc. Am.* **171**, 333–351.
Dean, S. L., Kulander, B. R. & Skinner, J. M. 1988. Structural chronology of the Alleghenian orogeny in southeastern West Virginia. *Bull. geol. Soc. Am.* **100**, 299–310.
Delphia, J. G. & Bombolakis, E. G. 1988. Sequential development of a frontal ramp, imbricates, and a major fold in the Kemmerer region of the Wyoming thrust belt. In: *Geometries and Mechanisms of Thrusting, with Special Reference to the Appalachians* (edited by Mitra, G. & Wojtal, S.). *Spec. Pap. geol. Soc. Am.* **222**, 207–222.
Dinares, J., McClelland, E. & Santanach, P. 1992. Contrasting rotations within thrust sheets and kinematics of thrust tectonics as derived from paleomagnetic data: an example from the Southern Pyrenees. In: *Thrust Tectonics* (edited by McClay, K. R.). Chapman & Hall, 265–275.
Dixon, J. S. 1982. Regional synthesis, Wyoming salient of the western overthrust belt. *Bull. Am. Ass. Petrol. Geol.* **66**, 1560–1580.
Evans, M. A. 1989. The structural geometry and evolution of foreland thrust systems: northern Virginia. *Bull. geol. Soc. Am.* **101**, 96–105.
Fletcher, R. C. & Pollard, D. D. 1981. Anticrack model for pressure solution surfaces. *Geology* **9**, 419–424.
Friedman, M. & Stearns, D. W. 1971. Relations between stress inferred from calcite twin lamellae and macrofractures, Teton Anticline, Wyoming. *Bull. geol. Soc. Am.* **82**, 3151–3162.
Gardener, D. A. C. & Spang, J. H. 1973. Model studies of the displacement transfer associated with overthrust faulting. *Bull. Can. Petrol. Geol.* **21**, 534–552.
Geiser, P. & Sansone, S. 1981. Joints, microfractures, and the formation of solution cleavage in limestone. *Geology* **9**, 280–285.
Goldberg, B. L. 1984. Displacement transfer between thrust faults near the Sun River in the Sawtooth Range, northwestern Montana. *Mont. geol. Soc. 1984 Field Conference*, 211–220.
Groshong, R. H. 1972. Strain calculated from twinning in calcite. *Bull. geol. Soc. Am.* **83**, 2025–2038.
Groshong, R. H. 1974. Experimental test of least squares strain gauge calculation using twinned calcite. *Bull. geol. Soc. Am.* **85**, 1855–1864.
Imlay, R. W. 1967. Twin Creek Limestone (Jurassic) in the western interior of the United States. *Prof. Pap. U.S. Geol. Surv.* **540**.
Jolly, A. D. & Sheriff, S. D. 1992. Paleomagnetic study of thrust sheet motion along the Rocky Mountain front in Montana. *Bull. geol. Soc. Am.* **104**, 779–785.
Kamb, B. 1959. Ice petrofabric observations from Blue Glacier, Washington, in relation to theory and experiment. *J. geophys. Res.* **64**, 1891–1909.
Kilsdonk, B. & Wiltschko, D. V. 1988. Deformation mechanisms in the southeastern ramp region of the Pine Mountain block, Tennessee. *Bull. geol. Soc. Am.* **100**, 653–664.
Kilsdonk, B. & Fletcher, R. C. 1989. An analytical model of hanging-wall and footwall deformation at ramps on normal and thrust faults. *Tectonophysics* **163**, 153–168.
Lageson, D. R. 1984. Structural geology of the Steward Peak Culmination, Idaho–Wyoming thrust belt. *Bull. Am. Ass. Petrol. Geol.* **68**, 401–416.
Lamerson, P. 1982. The Fossil Basin area and its relationship to the Absaroka fault system. In: *Geologic Studies of the Cordilleran Thrust Belt, Vol 1* (edited by Powers, R. B.). *Rocky Mtn. Ass. Geol.* 279–340.
Love, J. D. & Christiansen, A. C. 1985. Geologic Map of Wyoming. U.S. Geol. Surv. Map G85135.
Marshak, S. & Mitra, G. 1988. *Basic Methods of Structural Geology*. Prentice-Hall, Englewood Cliffs, New Jersey.
McCaskey, M. D. 1982. Deformation associated with transverse thrust ramps: a field and experimental study. M.S. thesis, Texas A&M University.
Mitra, G. & Yonkee, W. A. 1985. Relationship of spaced cleavage to folds and thrust in the Idaho–Utah–Wyoming thrust belt. *J. Struct. Geol.* **7**, 361–373.
Mitra, S. 1988. Three-dimensional geometry and kinematic evolution of the Pine Mountain thrust system, southern Appalachians. *Bull. geol. Soc. Am.* **100**, 72–95.
Moffat, I. W. & Spang, J. H. 1984. Origin of transverse faulting, Rocky Mountain Front Ranges, Canmore, Alberta. *Bull. Can. Petrol. Geol.* **32**, 147–161.
Oriel, S. S. & Platt, L. B. 1980. Geologic Map of the Preston 1 X 2 Quadrangle, Southeastern Idaho and Western Wyoming. U.S. Geol. Surv. Map I-1127.
Pfiffner, O. A. 1981. Fold and thrust tectonics in the Helvetic Nappes (E. Switzerland). In: *Thrust and Nappe Tectonics* (edited by McClay, K. R. & Price, N. J.). *Spec. Publ. geol. Soc. Lond.* **9**, 319–328.
Royse, F., Warner, M. & Reese, D. 1975. Thrust belt structural geometry and related stratigraphic problems in Wyoming, Idaho, and northern Utah. *Rocky Mtn. Ass. Geol. 1975 Symposium*, 41–54.
Rubey, W. W., Oriel, S. S. & Tracey, J. I. 1980. Geologic Map and Structure Sections of the Cokeville 30-Minute Quadrangle, Lincoln and Sublette Counties, Wyoming. U.S. Geol. Surv. Map I-1129.
Sorby, H. C. 1908. On the application of quantitative methods to the structure and history of rocks. *Q. J. geol. Soc. Lond.* **64**, 171–233.
Spang, J. H. & Brown, S. P. 1981. Dynamic analysis of a small imbricate thrust, and related structures, Front Ranges, southern Canadian Rocky Mountains. In: *Thrust and Nappe Tectonics* (edited by McClay, K. R. & Price, N. J.). *Spec. Publ. geol. Soc. Lond.* **9**, 143–150.
Spang, J. H., Wolcott, T. L. & Serra, S. 1981. Strain in the ramp regions of two minor thrusts, southern Canadian Rocky Mountains. In: Mechanical behavior of crustal rocks (edited by Carter, N. L., Friedman, M., Logan, J. M. & Stearns, D. W.). *Geophys. Mon. Am. Geophy. Union* **24**, 243–250.
Srivastava, D. C. & Engelder, T. 1990. Crack propagation sequence and pore fluid conditions during fault-bend folding in the Appalachian Valley and Ridge, central Pennsylvania. *Bull. geol. Soc. Am.* **102**, 116–128.
Wheeler, R. L. 1980. Cross-strike structural discontinuities: possible exploration tool for natural gas in the Appalachian overthrust belt. *Bull. Am. Ass. Petrol. Geol.* **64**, 2166–2178.
Wilkerson, M. S., Medwedeff, D. A. & Marshak, S. 1991. Geometrical modeling of fault-related folds: a pseudo-three-dimensional approach. *J. Struct. Geol.* **13**, 801–812.
Wilkerson, M. S., Marshak, S. & Bosworth, W. 1992. Computerized tomographic analysis of displacement trajectories and three dimensional fold geometry above oblique thrust ramps. *Geology* **20**, 439–442.
Wiltschko, D. V. 1979. A mechanical model for thrust sheet deformation at a ramp. *J. geophys. Res.* **84**, 1091–1104.
Wiltschko, D. V. & Dorr, J. A. 1983. Timing and deformation in overthrust belt and foreland of Idaho, Wyoming and Utah. *Bull. Am. Ass. Petrol. Geol.* **67**, 1304–1322.
Wiltschko, D. V., Medwedeff, D. A. & Millson, H. E. 1985. Distribution and mechanisms of strain within rocks on the northwest ramp of the Pine Mountain Block, southern Appalachian foreland: a field test of theory. *Bull. geol. Soc. Am.* **96**, 426–435.